Waste Biomass Valor
DOI 10.1007/s12649-013-9287-y

ORIGINAL PAPER

Stabilisation and Microstructural Modification of Stainless Steel Converter Slag by Addition of an Alumina Rich By-Product

Remus Ion Iacobescu · Annelies Malfliet · Lieven Machiels · Peter Tom Jones · Bart Blanpain · Yiannis Pontikes

Received: 16 August 2013 / Accepted: 23 December 2013

Abstract This work aimed to assess the possibility of stabilising argon oxygen decarburisation (AOD) stainless steel slag with $CaO/SiO_2 \sim 1.6$, by using a secondary alumina by-product ($\sim$75 wt% Al_2O_3, referred herein as SA, found under the name "Valoxy®") and reduced levels of B_2O_3. Two groups of samples were synthesised: one reference group with AOD slag and 0.26, 0.16, 0.10 and 0.05 wt% of B_2O_3 and one with equivalent compositions but to which 5 wt% of SA is added. Experimentally, the slags were produced in a platinum crucible in a resistance furnace, heated with 5 °C/min until 1,640 °C, equilibrated for 1 h, followed by slow cooling to room temperature. The mineralogical composition was analysed by QXRD whereas the micro-hardness was measured through a Vickers indentation test. The microchemistry and morphology were analysed by EPMA–WDS. Analysis indicated that AOD was successfully stabilised by 5 wt% SA and 0.10 wt% B_2O_3, whereas for 0.05 wt% B_2O_3, volumetric expansion occurred over time. In terms of mineralogy, the use of SA promoted the formation of spinel instead of gehlenite. Electron microscopy revealed a more dense morphology in the samples with SA when compared to the reference ones. Elemental maps indicated that Cr predominantly participates in the spinel phase. Vickers tests showed a slight increase in hardness in the samples with SA. In conclusion, the addition of SA resulted in substantially different microstructures that appear to be promising in terms of chemical and mechanical stability. However, in terms of volumes the required addition levels for effective stabilisation are substantial compared to B_2O_3 additions.

Keywords AOD slag · Volumetric stabilisation · Secondary alumina by-product · Reduced boron additions

R. I. Iacobescu (✉) · A. Malfliet · L. Machiels · P. T. Jones · B. Blanpain · Y. Pontikes
Department of Metallurgy and Materials Engineering, KU Leuven, 3001 Heverlee, Belgium
e-mail: remusion.iacobescu@mtm.kuleuven.be

Introduction

During argon oxygen decarburisation (AOD) of stainless steel in an AOD converter, AOD slag is generated. The slag contains CaO, SiO_2 and MgO as major oxides. Elements such as Cr, Al, Mn, Ni and Fe are present in minor quantities. The CaO/SiO_2 ratio varies between different steel plants and different AOD heats in the same plant but lies typically between 1.5 and 2.0. The major issue arising during AOD slag cooling is the high level of C_2S, a mineral which undergoes several phase transformations during cooling. The most important is the transition from β-C_2S (monoclinic) to γ-C_2S (orthorhombic) accompanied by a volume increase of around 12 % [1], resulting in a disintegration of the slag, the so-called "dusting effect". Because of the dusting, slag handling and storage becomes demanding. The Cr content in the slag is also a point of attention. In view of its effect to both humans and the environment, there is tight legislation regarding Cr VI leaching. Still, Cr III is rarely oxidised to Cr VI and in a number of cases it is entrapped in the spinel phase. In most cases, even for electric arc furnace (EAF) stainless steel slag which has a rather high Cr content [2] typically around 4–7 wt% "Cr_2O_3", leaching is not a major problem and the slag is used as an aggregate.

To avoid γ-C_2S and to reduce potential Cr leaching, two effective methods are usually followed: for the former, stabilisation of β-C_2S through addition of stabilising

Published online: 04 January 2014

compounds [3, 4] (e.g. B^{3+}), and for both the former and the latter, changing the ternary system $CaO–SiO_2–MgO$ towards a quaternary system with Al_2O_3 (e.g. by adding pure or secondary sources rich in Al_2O_3) [5]. A combination of the two methods is also possible. Another possibility could be the addition of MgO [6] in order to form a magnesiochromite spinel phase ($MgCr_2O_4$), or the addition of spinel compounds, as reported elsewhere [7]. These methods could effectively transform the slag and make it compliant with stringent environmental regulations.

Different materials are commercially available as a boron source, although boron wastes could also be used effectively [8]. Typically, only additions in low quantity are required, which permits their addition during tapping, with no external heating step needed. Nevertheless, despite the efficiency of the process, environmental concerns regarding boron leaching are expressed and alternative paths for slag stabilisation are investigated [9].

Slag stabilisation by Al addition could be such a path forward. The use of metallic Al is discouraging in view of its cost. Nevertheless, bauxites, kaolin clay, oil shales, coal waste, anorthosite etc. could be viable, low-cost alternatives [10]. Aluminium dross or salt cakes could also be interesting options [11]. All these secondary sources are in line with an industrial symbiosis perspective.

In the work of Mudersbach et al. [12], additions of bauxite, Al_2O_3 containing residues and aluminium metal were investigated as a method to increase the stability of stainless steel EAF slags and to stabilise Cr. The aim of the additions was to decrease the basicity of the slags, to favour the formation of spinel type phases during solidification and to avoid C_2S formation. Their work showed that there is a correlation between the so-called spinel factor and the actually measured Cr leaching levels, which seems to confirm that spinel behaves, in practice, as a stable phase with respect to chromium leaching. By performing a multivariate statistical analysis on a large number of industrial stainless steel EAF slags, they correlated the level of Cr leaching to the concentration of spinel forming compounds in the slag. The obtained empirical formula is called the factor SP:

$$SP = 0.2 \cdot MgO + 1.0 \cdot Al_2O_3 + n \cdot FeO_x - 0.5 \cdot Cr_2O_3$$

with 'n' a number between 1 and 4, depending on the oxidation state of the slag. When the factor sp exceeded 5 wt%, Cr leaching fell below the German norm of 0.05 mg/l Cr in the leachate. In other studies [13, 14], the additions of Al_2O_3 (3–12 wt%) to a slag basicity of 1.6 was shown to significantly increase the spinel formation and the Cr in the spinel phase decreased as a function of Al_2O_3 addition. Tossavainen and Forssberg [15] showed that the addition of spinel forming compounds, such as MgO, Al_2O_3 and FeO, to the slag at high temperature does in fact decrease the level of Cr leaching. In a work also related to Al additions, Stubbe et al. [16] recently reported their results on aluminium injection to EAF slags. After the successful operational trials, Al injection was industrially applied at the BGH stainless steel plant with important benefits such as high Cr recovery in the steel and low total Cr level in the slag with a final chemistry close to calcium aluminate cements.

In contrast, to the best of our knowledge, the addition of Al rich by-products or residues for AOD slag stabilisation has not been investigated. This study, therefore, explores the use of a secondary source of alumina for the stabilisation of AOD slag with variable, preferably reduced, boron oxide additions. The central focus is placed on the mineralogical composition and microstructure of SA stabilised AOD slags. The motivation was to investigate whether it is possible to produce a better slag quality in terms of physical, mechanical or environmental behaviour. The envisaged volumetrically stable slag can be either safely disposed or can find application as aggregate in concrete or asphalt. Compared to a non-stabilised slag and depending on the final microstructure that is achieved, the new slag is expected to be dense, with Cr incorporated in crystalline phases. Considering Cr will be both physically and chemically bound, the leaching is expected to be minimized. In addition to the above, the handling of the slag will be facilitated with no release of airborne particles. Compared to presently boron-stabilised slags, the new slag is expected to have less boron and better Cr leaching characteristics.

Materials and Methods

The raw materials used in this project were a secondary alumina source (referred herein as SA, found under the name "Valoxy®" from RVA, France), AOD slag and disodium tetraborate (DT, $Na_2B_4O_7$) as a source of boron oxide. SA is a product rich in alumina (i.e. ~75 wt%) arising from the re-treatment of salt slags, drosses and general dusts from the aluminium industry. Its main components are corundum, magnesium spinel and boehmite or diaspore [17]. DT is a commercially available product and contains approx. 69 wt% B_2O_3 and 31 wt% Na_2O. Prior to XRF and XRD/QXRD characterisation, the raw materials, SA and AOD slag, were dried at 100 °C until a constant weight was reached and then milled into a fine powder using a Retsch centrifugal mill with sieve opening 80 μm. For XRD/QXRD analysis, the powdered materials were further milled with a McCrone Micronising mill®, in presence of 10 wt% ZnO as internal standard and 5 ml of ethanol as grinding agent, for a 5 min period in order to identify the amorphous content. After drying, the sample

was homogenised in a mortar crusher. XRF analysis was performed using a Philips PW2400 spectrometer. X-ray (XRD) diffraction patterns were measured using a Philips PW1830 diffractometer over a 2θ range of 10°–70° using CuKα radiation of 40 kV and 35 mA, a 0.02° step size and step time of 2 s, with spin on. Quantitative results (QXRD) were obtained adopting the Rietveld method [18, 19], using the "Topas® Academic" software [20]. A fundamental parameter approach was used, meaning that instrumental contributions to the peak shapes were calculated directly [21] and the standard parameters (cell parameters, crystallite size, lattice strain, diffraction optical effects and background) were refined.

FactSage calculations were used to predict the required level of SA to avoid C_2S formation above 5 wt% and to see the effect on mineralogy. The analysis was performed with the FactSage software using the databases FS-Stel and FT-Oxid. To verify the calculations, AOD modified slag was produced and investigated visually and by XRD/QXRD.

For producing the modified slag, a bottom loading furnace (AGNI ELT 160-02) was used. Each sample was heated until 1,640 °C at 5 °C/min, equilibrated for 1 h, followed by slow cooling at 5 °C/min to room temperature, in a platinum crucible. The experiments took place in atmospheric conditions. For the preliminary investigation three sets of samples were produced, with 15, 10 and 5 wt% SA and no boron oxide addition, named as SA15, SA10 and SA5. For the final investigation, four samples were produced by adding 5 wt% SA and reduced boron oxide (B_2O_3) additions of 0.26 wt% (SA5B26), 0.16 wt% (SA5B16), 0.10 wt% (SA5B10) and 0.05 wt% (SA5B05). Another set of four samples was produced for comparison, adding only B_2O_3 in the same amounts and no SA. These were named respectively B26, B16, B10 and B05.

After solidification, the first characterisation of the samples was visual inspection, followed by EPMA–WDS analysis and Vickers micro-hardness measurements for the stable slags (after 2 days of storage in open air). XRD/QXRD characterisation was done on all samples. For macroscopical images a photo camera (Canon IXUS 85 IS) was employed. XRD/QXRD analysis was done on samples prepared by using a McCrone Micronising mill® in order to avoid any effect on crystal morphology and/or preferred orientation during grinding [22]. A similar device and parameters as presented above (Philips PW1830 diffractometer) was employed. For microchemistry and morphology characterisation by fully quantitative EPMA–WDS (using high purity reference standards), cylindrical samples were sampled by using a diamond coated drill. The extracted cylindrical samples were then embedded in Epoxy resin and polished successively with SiC abrasive paper down to P2400 (P-grade) grit. As a final step, a TexMet® 1,500 cloth disc was used with MetaDi® Diamond paste for polishing, followed by carbon coating. Vickers micro-hardness (HV_1) tests were done on embedded polished samples. At least 10 points were measured on each sample surface and the average values were reported.

Results and Discussion

Raw Materials Characterisation

The XRF results on the raw materials are presented in Table 1, whereas the QXRD results can be found in Table 2. AOD slag is rich in CaO, SiO_2 and MgO in higher percentages. The C/S ratio equals ~1.6 (Ca from CaF_2 excluded). Small amounts of Al_2O_3, Fe_2O_3, MnO and Cr_2O_3 were also found. SA contains mainly Al_2O_3 (~75 wt%), followed by MgO and SiO_2 in minor amounts. Elements such as Ca, Fe, Ti, K, Cu, Na, Mn and S are present in minor quantities, below 1–2 wt% when expressed as oxides. The mineralogical composition of AOD slag is rich in Mg/Si and Ca/Si phases, such as merwinite (22 wt%), bredigite (18 wt%), cuspidine (21 wt%) and γ-C_2S (20 wt%). In lower amounts, periclase (8 wt%), β-C_2S (7 wt%) and wollastonite (2 wt%) were also found. As regards to SA, a high amorphous content of about 55 wt% was identified. The main crystalline phases are spinel (12 wt%), corundum (8 wt%), boehmite (4.4 wt%), Cu-spinel (3.2 wt%), bayerite (3 wt%) and aluminium (1.6 wt%). Other crystalline phases (below 1.5 wt%) were also present and amount to ~11 wt% of the total content. These are quartz, calcite, pyrolusite, nordstrandite, halite, periclase, elpasolite, diaspore, microcline, rutile, fluorite, magnetite, silicon, gypsum and goethite. The Al_2O_3 content in SA will act as a system modifier for AOD slag,

Table 1 XRF characterization of AOD slag and SA raw materials, in wt%

Oxides	AOD slag	Oxides	SA
CaO	55.7	Al_2O_3	75.8
SiO_2	33.0	MgO	9.2
MgO	7.6	SiO_2	7.2
Al_2O_3	1.3	CaO	1.9
Cr_2O_3	0.7	Fe_2O_3	1.4
MnO	0.4	TiO_2	0.8
Fe_2O_3	0.3	K_2O	0.8
		CuO	0.5
		Na_2O	0.5
		MnO	0.4
		SO_3	0.3
		Cl^-	0.6
Total	99.0	Total	99.4

Table 2 QXRD characterization of AOD slag and SA, in wt%

Identified minerals	AOD slag	Identified minerals	SA
Merwinite ($Ca_3Mg(SiO_4)_2$)	22.4	Spinel ($MgAl_2O_4$)	12.0
Cuspidine ($Ca_4Si_2O_7F_2$)	21.2	Corundum (Al_2O_3)	8.8
γ-C_2S (Ca_2SiO_4)	20.3	Boehmite (α-AlO(OH))	5.2
Bredigite ($Ca_7Mg(SiO_4)_4$)	18.0	Cu-Spinel $(Cu,Mg)Al_2O_4$)	3.2
Periclase (MgO)	8.1	Bayerite ($Al(OH)_3$)	3.0
β-C_2S (Ca_2SiO_4)	7.5	Aluminium (Al)	1.6
Wollastonite ($CaSiO_3$)	2.1	Others[a]	11.0
Fluorite (CaF_2)	0.3	Amorphous	55.2
Total	100	Total	100

[a] Others include, in wt%: Quartz (SiO_2)—1.4, Calcite ($CaCO_3$)—1.4, Pyrolusite (MnO)—0.4, Nordstrandite ($Al(OH)_3$)—1.2, Halite (NaCl)—1.2, Periclase (MgO)—0.9, Elpasolite (K_2NaAlF_6)—0.9, Diaspore (AlO(OH))—0.8, Microcline ($KAlSi_3O_8$)—0.7, Rutile (TiO_2)—0.8, Fluorite (CaF_2)—0.4, Magnetite (Fe_3O_4)—0.2, Silicon (Si)—0.2, Gypsum ($CaSO_4{\cdot}2H_2O$)—0.2, Goethite (FeO(OH))—0.3

leading to a transition from a ternary CaO–SiO_2–MgO to a quaternary CaO–SiO_2–MgO–Al_2O_3 slag system, diminishing the formation of the unwanted (γ) polymorphic form of C_2S phase [5]. Moreover, by mixing AOD with SA, the SiO_2 provided to the system by the latter will decrease the Ca/Si ratio of AOD slag and reduce the need of high amounts of Al_2O_3. The presence of spinel in SA is an interesting aspect as it may act as a Cr bounding phase already from lower temperature, or even, as a nucleating site promoting further spinel crystal growth [6].

Preliminary Investigations

The FactSage thermodynamic calculations of SA additions to AOD slag and of temperature drop when SA is added to AOD slag at ~1,600 °C, are presented in Figs. 1 and 2, respectively. In Fig. 3 is given the FactSage thermodynamic equilibrium cooling diagram of 15 wt% SA addition

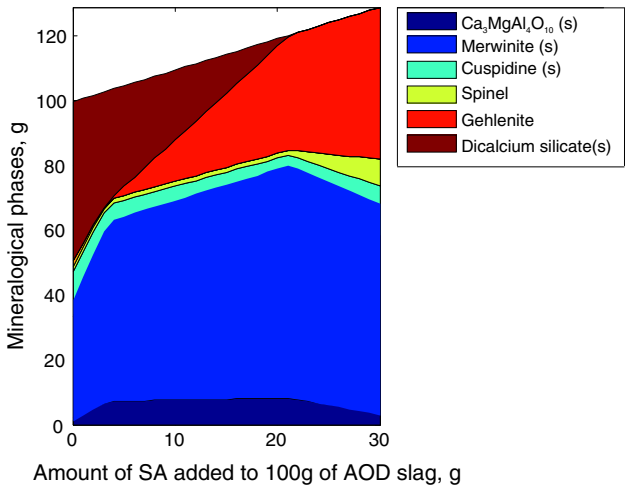

Fig. 1 FactSage thermodynamic calculations of SA addition to AOD slag, predicting the phases formed upon cooling at 700 °C

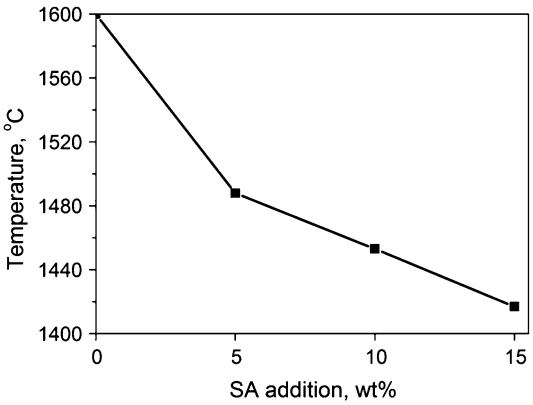

Fig. 2 FactSage thermodynamic calculations of temperature drop when 5, 10 and 15 wt% of SA (25 °C) is added to the AOD slag at high temperature

to the AOD slag. Macroscopical images of AOD modified slag with SA additions are presented in Fig. 4, whereas the results from the QXRD characterization are given in Table 3. From the FactSage calculation it can be estimated that for a basicity of ~1.6, about 15 wt% (17 %) of SA (17 g of SA to 100 g of slag) is sufficient for stabilisation, assuming that the AOD slag is becoming un-stable when the γ-C_2S content is ~4 wt%. It has been estimated that for a basicity of ~2.0, about 23 wt% of SA addition is needed for stabilisation. Industrially, this is quite challenging. Typically, materials to be added are not preheated and a temperature drop is thus expected when SA is introduced in the melt. A way to mitigate this would be by concurrent addition of a heat generating agent (e.g. FeSi). When 15 wt% is added the temperature drops by 180 °C approximately (Fig. 2), whereas by adding 10 or 5 wt% the temperature drop is around 150 and 110 °C, respectively. In Fig. 3 it can be seen that, for the basicity of ~1.6 used in this study, at 1,600 °C part of the slag is molten with α-C_2S also present. At lower temperature, spinel is the first

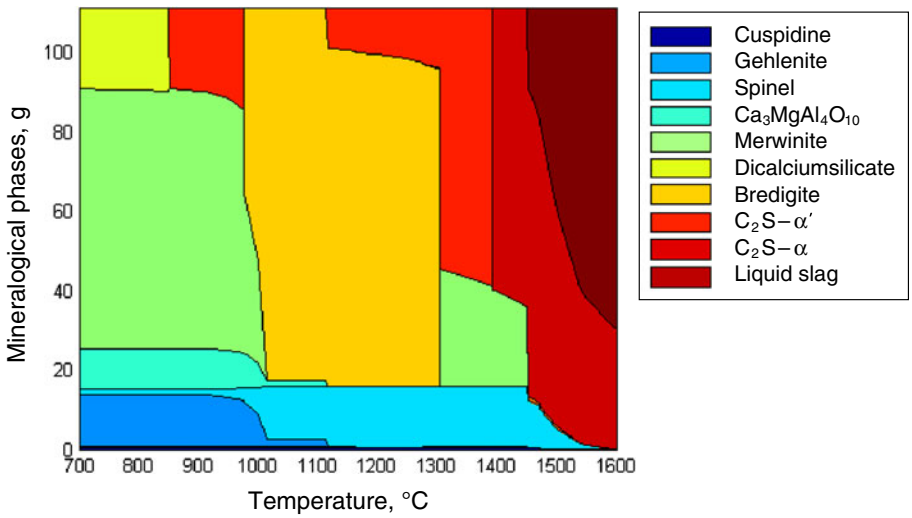

Fig. 3 FactSage thermodynamic equilibrium cooling calculations of 15 wt% SA (17 g) addition to AOD slag, predicting the phases formed upon cooling from 1,600 °C at 700 °C

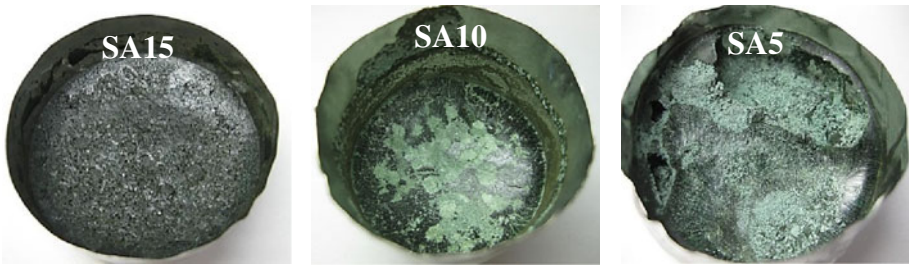

Fig. 4 Macroscopical images of AOD modified slag with SA addition

Table 3 Quantitative analysis of samples with SA addition, in wt%

Identified minerals	SA15	SA10	SA5
Merwinite	45.7	42.4	40.2
Bredigite	14.4	18.0	27.0
Gehlenite	14.1	6.7	1.9
Spinel	12.2	13.0	6.1
Cuspidine	4.4	5.0	3.3
Periclase	2.6	3.5	5.3
γ-C_2S	1.9	3.9	4.4
Lime	0.3	0.2	0.0
Fluorite	0.5	1.5	1.6
Calcite	0.3	0.0	0.0
Wollastonite	0.7	2.5	5.1
β-C_2S	2.8	3.0	5.0
	Stable	Un-stable	Un-stable

phase to precipitate, followed by merwinite and α′-C_2S. The formation of bredigite initiates around 1,300 °C, whereas $Ca_3MgAl_4O_{10}$ and gehlenite form below 1,100 °C. The last phase precipitating is C_2S with α'-polymorphic form which transforms to β-polymorphic form when the temperature drops below 900 °C. For a temperature <700 °C, no further changes are expected to take place considering the very slow kinetics. Thus, at room temperature, C_2S, merwinite, $Ca_3MgAl_4O_{10}$, spinel and gehlenite are expected to be the final phases.

From the macroscopical characterisation (Fig. 4) it was observed that the experiment with SA addition of 15 wt% was successful. As the SA addition was decreased to 10 wt% (SA10) and 5 wt% (SA5), the slag became unstable.

For SA addition to AOD slag, the final phases detected after solidification were mainly merwinite, bredigite, gehlenite (except for SA5) and spinel (Table 3). The presence of merwinite and bredigite is probably due to the presence of SiO_2 and MgO provided by SA. Minerals like cuspidine, periclase, γ-C_2S, β-C_2S, fluorite and wollastonite have also been identified in lower amounts. With decreasing SA addition, the γ-C_2S increases together with the instability of the slag; the relevant values of γ-C_2S are: 1.9, 3.9 and 4.4 wt% for 15, 10 and 5 wt% SA addition, respectively. The content of spinel has also changed with decreasing SA addition. It is found that $MgAl_2O_4$ spinel type formation is more favoured instead of gehlenite at low alumina levels available in the system. Part of the spinel probably originates from SA (content in bulk in $MgAl_2O_4$ type spinel phase is around 12 wt%) as its melting point is at about 2,100 °C [23], which is higher than the experimental temperature (1,640 °C). Yet, the important fraction is formed upon cooling. The formation of spinel provides the

advantage of hosting Cr(III) in the crystal lattice and thus Cr leaching is expected to be low [6].

In view of the promising results of 15 wt% SA addition, and considering that this is a substantial amount, an alternative strategy was investigated where the sample with 5 wt% SA was combined with boron oxide. The goal was to investigate if the addition of SA can reduce the required boron oxide level and deliver a final slag with better microstructure. The resulting slag after solidification was studied.

Mineralogical Analysis of Produced Slags with Boron Oxide

The results of the QXRD characterisation are presented in Table 4. All samples were stable, except the one with the lowest boron oxide content (0.05 wt%). The samples with SA contain mainly merwinite, followed by bredigite, for all situations. For the benchmark samples without SA, bredigite is the main phase. Other differences relate mostly to gehlenite and spinel, being present in higher levels in the samples with SA. It seems that small amounts of gehlenite and spinel were formed in the reference samples after remelting and stabilisation with boron oxide as these do not appear in the mineralogical composition of the AOD slag. A comparison of AOD samples with 5 wt% SA with and without boron oxide addition reveals that γ-C_2S is responsible for the instability phenomenon. In the cases of boron oxide (B_2O_3) additions of 0.26, 0.16 and 0.10 wt%, only a small amount of γ-C_2S was encountered, without a negative effect on stability. As boron oxide addition decreased to 0.05 wt%, γ-C_2S was not avoided in both samples, with and without SA and the slag became unstable. It seems that a value close to 4 wt% γ-C_2S is enough to cause instability of the sample for the given basicity. This phenomenon was also seen in the preliminary investigation where the samples with 10 and 5 wt% SA addition became unstable with a content of γ-C_2S of about 4 wt% in the modified slag. All samples contain free MgO (periclase). A higher content was found in all samples without SA. This indicates a possible risk of volume expansion if exposed to wet environment due to the formation of magnesium hydration products, such as brucite.

Microchemical Analysis of Produced Slags with Boron Oxide

The BSE images of the stable AOD modified slag samples with 5 wt% SA with and without boron oxide addition are presented in Fig. 5. The results of the WDS point analysis on the main mineralogical phases identified are shown in Table 5. The elemental mappings of the samples with 5 wt% SA with and without 0.26 wt% boron oxide additions (B_2O_3) are shown in Fig. 6 (CP-Backscattered electron image of analysed area). All samples with SA demonstrated a smoother and dense microstructure with a larger amount of primary crystalline phase and without visible large pores, compared to the reference samples with boron oxide addition only (see Fig. 5). The former is dominated by gehlenite, spinel, merwinite and bredigite phases, whereas the latter contains more merwinite and bredigite and less spinel and gehlenite. In all samples with SA addition, a dendritic morphology (merwinite) is seen. The polymorphic form of β-C_2S was stabilised successfully by boron oxide additions and it was sporadically observed in samples with SA. A detailed image of a stabilised C_2S grain, most probably the beta polymorphic form due to the characteristic parallel striations stabilised upon cooling by boron oxide addition is shown in Fig. 7. The WDS analysis on this C_2S and the surrounding phases is given in the table attached to Fig. 7. The grain of β-C_2S is present in a roundish shape in most situations, with parallel twin

Table 4 Quantitative analysis of samples with and without SA and boron oxide additions, in wt%

Identified minerals	SA5B26	B26	SA5B16	B16	SA5B10	B10	SA5B05
Merwinite	52.7	23.7	42.3	17.2	41.1	15.1	44.2
Bredigite	18.5	49.7	32.7	56.8	33.4	59.6	25.1
Spinel	6.7	1.7	5.0	1.2	6.1	1.1	5.4
β-C_2S	6.3	4.4	5.3	5.4	5.8	5.8	5.5
Periclase	2.4	6.0	4.0	6.7	3.2	7.7	3.4
Gehlenite	3.9	0.8	1.6	0.4	0.8	0.3	2.0
Calcite	3.6	2.5	3.0	2.8	4.0	2	4.4
Fluorite	2.0	0.8	1.3	0.9	1.5	1.0	1.7
γ-C_2S	0.3	1.2	1.5	0.4	1.0	0.4	3.6
Cuspidine	2.6	7.0	2.0	5.7	2.3	4.4	3.1
Quartz	0.7	1.4	0.8	1.1	0.9	0.9	0.7
Wollastonite	0.6	0.8	0.5	1.4	0.0	1.7	1.0
	Stable						Partly un-stable

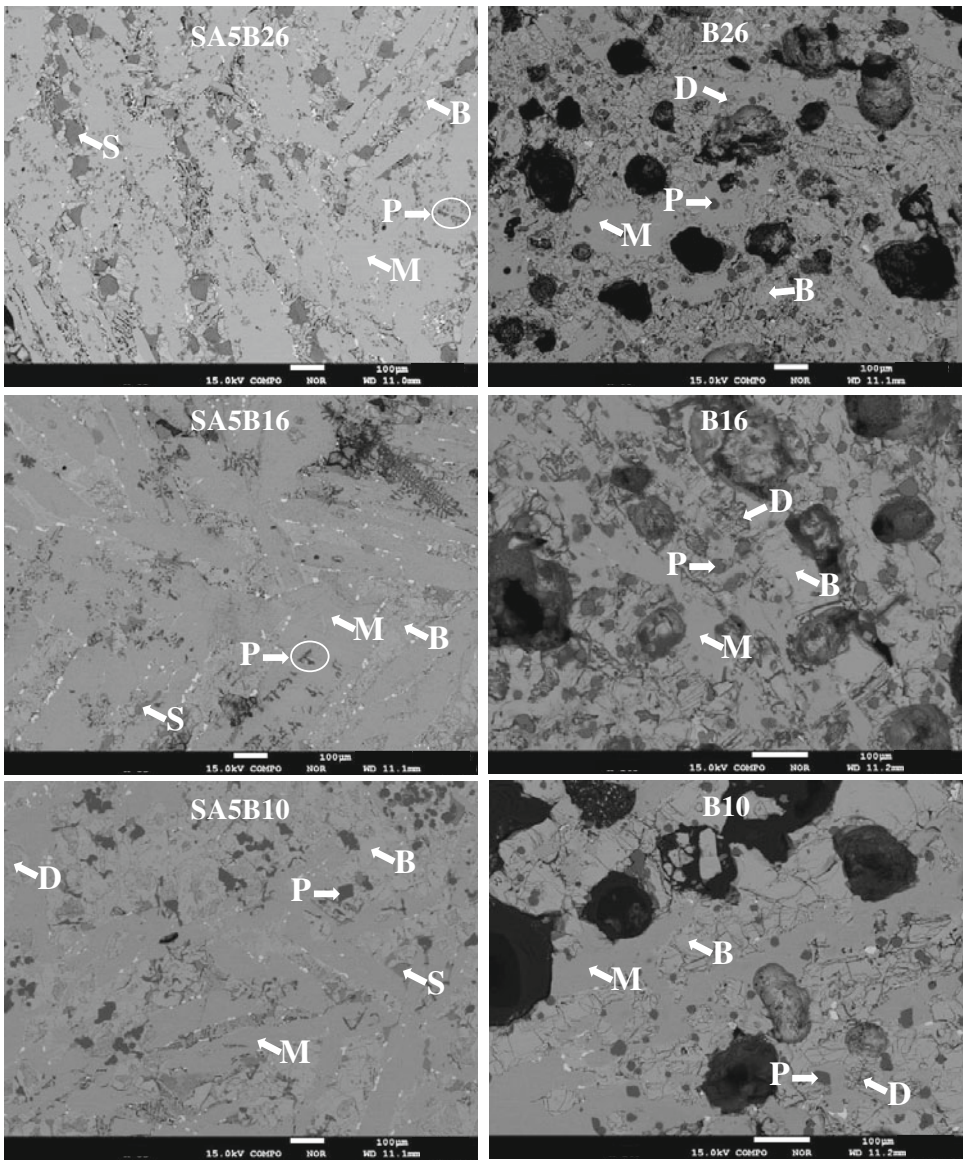

Fig. 5 Backscattered electron (BSE) images of a sectioned polished surface of the produced stable samples with/without SA and boron oxide additions. The main minerals identified on the images are: *B* bredigite, *M* merwinite, *P* periclase, *S* spinel, *D* dicalcium silicate

Table 5 WDS point microanalyses on the main mineralogical phases identified in samples with/without SA and boron oxide addition. The average and standard deviation is reported, in wt%

Samples	Minerals	Oxides (average ± standard deviation)				
		Al_2O_3	MgO	CaO	SiO_2	Cr_2O_3
AOD + 5 wt% SA and boron oxide additions	Merwinite	0.2 ± 0.0	11.6 ± 0.3	51.8 ± 1.0	33.6 ± 1.4	0.2 ± 0.1
	Bredigite	0.3 ± 0.1	5.4 ± 0.2	57.6 ± 1.4	30.5 ± 0.8	0.3 ± 0.1
	Spinel	59.9 ± 4.8	26.2 ± 0.6	0.5 ± 0.2	0.4 ± 0.2	5.4 ± 3.0
	β-C_2S	0.3 ± 0.1	0.3 ± 0.1	62.6 ± 3.8	33.4 ± 0.6	0.4 ± 0.1
AOD + boron oxide additions	Merwinite	0.1 ± 0.1	11.7 ± 0.2	52.0 ± 1.1	33.2 ± 0.2	0.2 ± 0.1
	Bredigite	0.2 ± 0.1	5.3 ± 0.1	57.6 ± 1.4	32.7 ± 2.9	0.3 ± 0.1
	β-C_2S	0.1 ± 0.0	0.3 ± 0.1	62.1 ± 5.4	30.3 ± 5.5	0.3 ± 0.1

lamellae, and surrounded respectively by bredigite and merwinite (Fig. 7), a microstructure reported also by others [24, 25]. An important part of the Cr content, introduced through the AOD slag, appears to be incorporated in the spinel phase, Table 5. Based on this observation, leaching is expected to be minimised as described elsewhere [15].

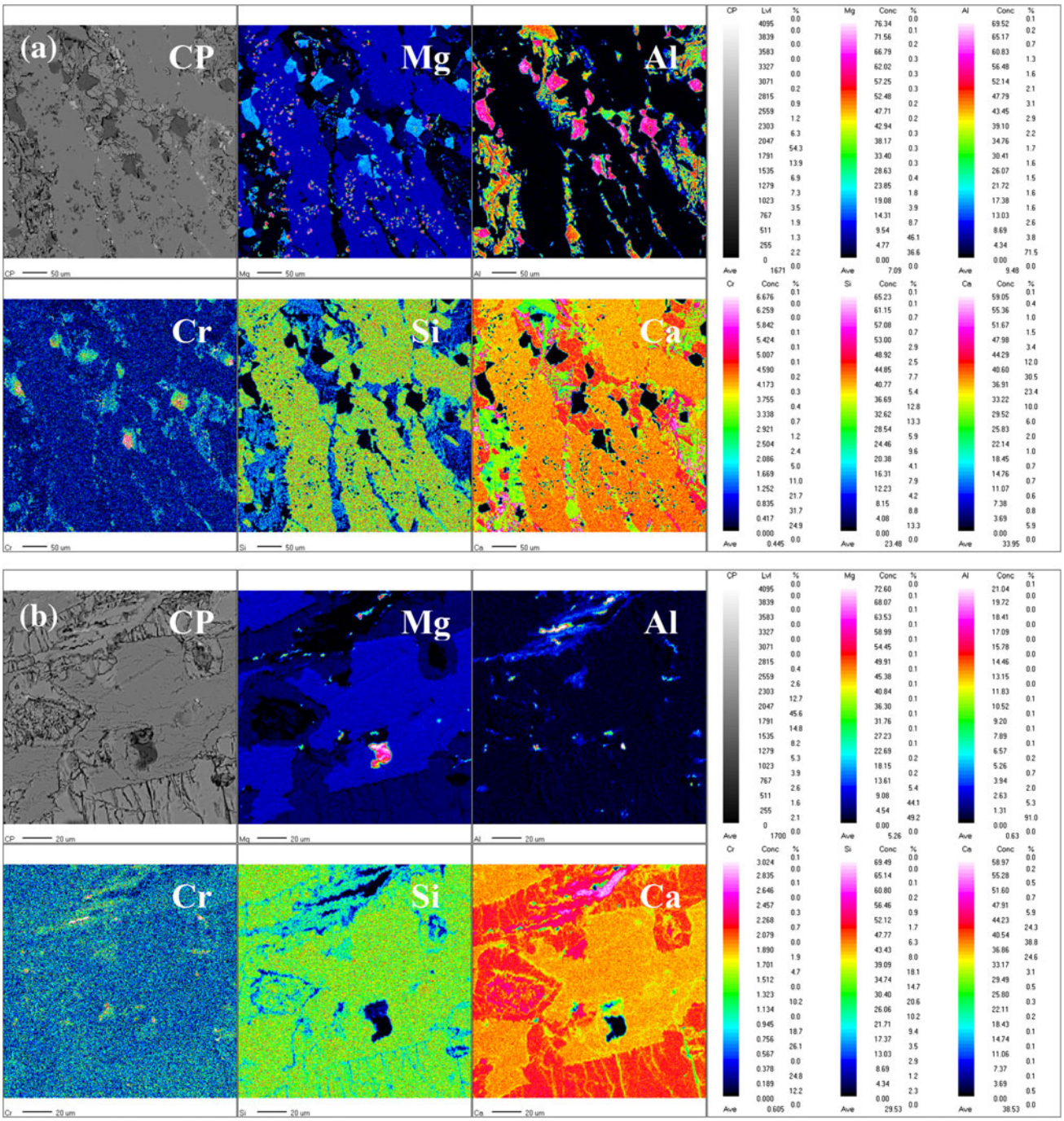

Fig. 6 EPMA–WDS mapping analysis of AOD modified slag samples: **a** V5B26 and **b** B26. The elements investigated are: Mg, Al, Cr, Si and Ca (CP-Backscattered electron image of analysed area)

Vickers Micro-Hardness Test of Produced Slags with Boron Oxide

The results of Vickers micro-hardness tests are presented in Fig. 8. Comparable average values were reached in all cases but with a standard deviation that is consistently substantially large. At least three factors contribute to the above, among others [26], (1) the ratio between the different crystalline phases, (2) the crystal growth of each phase, and (3) the porosity. This complexity is evident in Fig. 9 where the indentation area in a bredigite crystal surrounded by merwinite is shown. In this particular case, the indenter did not penetrate the merwinite and the periphery of the indentation area followed to some extent the crystal interfase between merwinite and the matrix. When the measurement was taken on a merwinite crystal,

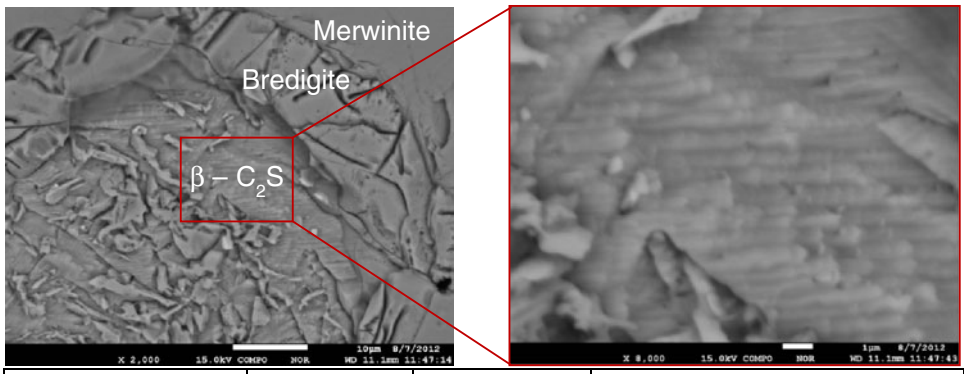

Fig. 7 BEI with WDS analysis on C_2S grain and the neighborhood composed of Bredigite and Merwinite phases

Oxides, wt%	Merwinite	Bredigite	β – Dicalcium silicate (C_2S)
CaO	53.18	61.21	66.84
SiO_2	34.33	32.58	32.63
MgO	11.96	5.61	0.11
Al_2O_3	0.04	0.09	0.02
Cr_2O_3	0.30	0.36	0.29

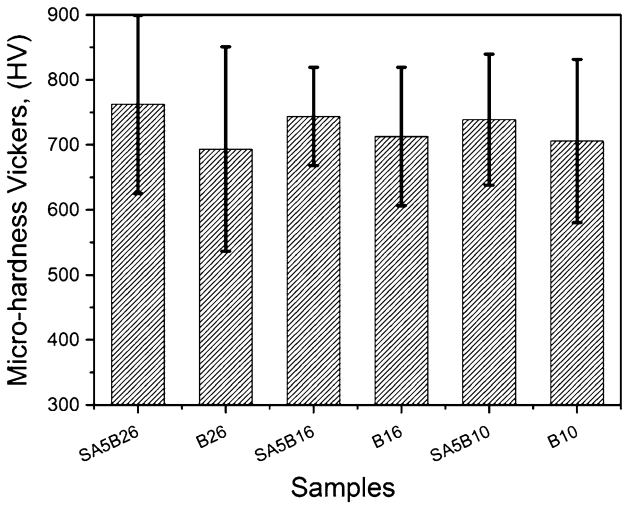

Fig. 8 Vickers micro-hardness (HV_1) tests results of samples with/without SA and boron oxide additions

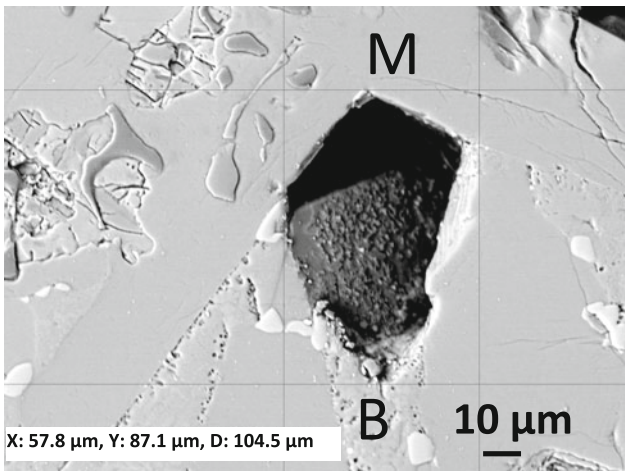

Fig. 9 SEM images of a sample after Micro-hardness test, showing the indentation area and shape in a bredigite crystal produced during testing. Abbreviations: *M* merwinite, *B* bredigite

the indentation area was always smaller compared to bredigite and radial cracking developing from the impression corners was also evident. The above are consistent with the Mohs scale of hardness, where merwinite has 6 [27] and bredigite 5.5 [28]. Despite the complexity, it is still interesting to note that addition of 5 wt% SA in the compositions seems to lead to higher average values, Fig. 8. This could be attributed to the higher ratio of merwinite to bredigite and the seemingly less porous microstructure in the mixtures with SA. A more thorough analysis of the microstructure is required and additional relevant information would have been obtained if compressive strength measurements could be performed. Due to the small quantity of sample produced this has not been possible.

Volumetric Stability

A summary of the volumetric stability is given in Fig. 10. Boron oxide additions down to 0.1 wt% proved to be efficient for the stabilisation of AOD slag independent of the presence of SA. The effectiveness of boron as a doping cation promoting the stabilisation of the β-polymorph is indeed not new [29, 30]. At 0.05 wt% B_2O_3 addition, the sample with SA became partially unstable. The instability starts to be visible after 1 day of storage, with slow disintegration over time. This phenomenon has been described in literature as "late falling" [31]. The threshold of stability-instability for the specific AOD slag tested with/without 5 wt% SA addition is between 0.10 and 0.05 wt%

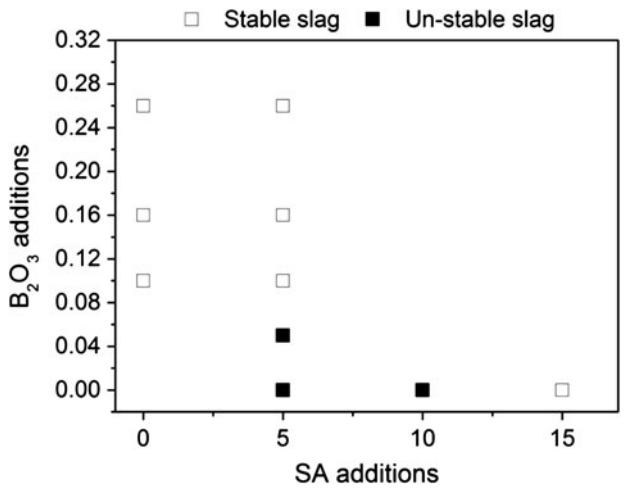

Fig. 10 Summary on the volumetric stability of slag as a function of equivalent B_2O_3 (DT) and SA addition

B_2O_3. It thus appears that the presence of minor levels of K and Na in SA, that in principle have the potential to contribute in the stabilisation of β-C_2S [3] had no practical consequence. Similarly, the more dense microstructure in the samples with SA, that also can promote the β-C_2S retention by exercising higher hydrostatic pressure on the C_2S grains [32], did not suffice alone or had a notable contribution in preventing the β to γ transformation.

Conclusions

The following core conclusions can be derived from this work:

- The volumetric stabilisation of AOD slag cooled at room temperature was possible by adding SA.
- Substantial additions (15 wt%) are required to prevent the C_2S formation and in effect stabilise the AOD slag. At lower amounts, the slag disintegrates due to the γ-C_2S formation. About 4 wt% of γ-C_2S in the final slag is sufficient to cause slag disintegration.
- The AOD slag with 5 wt% SA addition was successfully stabilised by boron oxide (B_2O_3) additions of 0.26, 0.16 and 0.10 wt%. Spinel formation was favoured instead of gehlenite, while merwinite is prevailing over bredigite. This is due to the MgO provided by SA.
- Addition of 5 wt% SA and reduced boron oxide additions to AOD slag delivered solidified materials with a more dense microstructure when compared with those stabilised from boron oxide addition only.
- Addition of 5 wt% SA promoted an extended formation of spinel phase and elemental mappings indicate that Cr is associated with it. According to other studies, Cr leaching is expected to be minimised. Leaching experiments should be conducted in order to verify the above.
- Vickers micro-hardness testing indicates that SA addition improves the hardness primarily due to a higher ratio of merwinite over bredigite.

Acknowledgments The financial support of RVA, France is gratefully acknowledged as well as the active involvement of Mr. H. Epstein. The thermodynamic calculations were performed by E. Nagels, InsPyro NV. The EPMA–WDS work has been feasible due to the support of the Hercules Foundation (Project ZW09-09). Yiannis Pontikes is thankful to the Research Foundation-Flanders for the post-doctoral fellowship.

References

1. Bridge, T.E.: Bredigite, larnite and dicalcium silicate from Marble Canyon. Am. Miner. **51**, 1766–1774 (1966)
2. Guo, M., Durinck, D., Jones, P.T., Heylen, G., Hendrickx, R., Baeten, R., Blanpain, B., Wollants, P.: EAF stainless steel refining—part I: observational study on chromium recovery in an eccentric bottom tapping furnace and a spout tapping furnace. Steel Res. Int. **78**(2), 117–124 (2007)
3. Taylor, H.F.W. (ed.): Cement Chemistry, 2nd edn. Academic Press, London (1990)
4. Pontikes, Y., Jones, P.T., Geysen, D., Blanpain, B.: Options to prevent dicalcium silicate-driven disintegration of stainless steel slags. Arch. Metall. Mater. **55**(4), 1167–1172 (2010)
5. Park, J.H.: Solidification structure of CaO–SiO_2–MgO–Al_2O_3 (–CaF2) systems and computational phase equilibria: crystallization of $MgAl_2O_4$ spinel. Calphad **31**(4), 428–437 (2007)
6. Engström, F.: Mineralogical Influence of Different Cooling Conditions on Leaching Behaviour of Steelmaking Slags. Luleå University of Technology, Luleå, Sweden (2007)
7. Durinck, D., Engström, F., Arnout, S., Heulens, J., Jones, P.T., Björkman, B., Blanpain, B., Wollants, P.: Hot stage processing of metallurgical slags. Resour. Conserv. Recycl. **52**(10), 1121–1131 (2008)
8. Pontikes, Y., Kriskova, L., Wang, X., Geysen, D., Arnout, S., Nagels, E.: Additions of industrial residues for hot stage engineering of stainless steel slags. In: Jones, P., Pontikes, Y., Elsen, J., Cizer, Ö., Boehme, L., Van Gerven, T. (eds.) 2nd International Slag Valorisation Symposium, pp. 313–326. Leuven, Belgium (2011)
9. Yoshinaga, J., Kida, A., Nakasugi, O.: Statistical approach for the source identification of boron in leachates from industrial landfills. J. Mater. Cycles Waste Manage. **3**(1), 60–65 (2001)
10. http://www.scienceviews.com/geology/aluminum.html
11. Tsakiridis, P.E.: Aluminium salt slag characterization and utilization—a review. J. Hazard Mater. **217–218**, 1–10 (2012). doi:10.1016/j.jhazmat.2012.03.052
12. Mudersbach, D., Kühn, M., Geisler, J., Koch, K.: Chrome immobilisation in EAF-slags from high-alloy steelmaking: tests at FEhS institute and development of an operational slag treatment process. In: Jones, P.T., Geysen, D., Guo, M., Blanpain, B. (eds.) First International Slag Valorisation Symposium. Leuven, Belgium (2009)
13. García-Ramos, E., Romero-Serrano, A., Zeifert, B., Flores-Sanchez, P., Hallen-Lapez, M., Palacios, E.G.: Immobilization of chromium in slags using MgO and Al_2O_3. Steel Res. Int. **79**(5), 332–339 (2008)

14. Galina Jelkina Albertsson: Investigations of Stabilization of Cr in Spinel Phase in Chromium-Containing Slags. KTH, Stockholm (2011)
15. Tossavainen, M., Forssberg, E.: Leaching behaviour of rock material and slag used in road construction—a mineralogical interpretation. Steel Res. **71**(11), 442–448 (2000)
16. Stubbe, G., Harp, G., Sedlemeier, M.: New technology for recovery of chromium from EAF stainless steelmaking slag. In: Waste Recovery in Ironmaking and Steelmaking Processes. The Institute of Materials, Minerals and Mining, London (2010)
17. www.rva-recycling.com. (Accessed in May 2013)
18. Rietveld, H.M.: A method for including the line profiles of neutron powder diffraction peaks in the determination of crystal structures. Acta Crystallogr. **21**, A228 (1966)
19. Rietveld, H.M.: A profile refinement method for nuclear and magnetic structures. J. Appl. Crystallogr. **2**, 65–71 (1969)
20. Coelho, A.A.: TOPAS-Academic; A Computer Programme for Rietveld Analysis. http://www.topas-academic.net/ (2004)
21. Cheary, R.W., Coelho, A.A.: A fundamental parameters approach of X-ray line-profile fitting. J. Appl. Crystallogr. **25**, 109–121 (1992)
22. Buhrke, V.E., Jenkins, R., Smith, D.K.: A practical guide for the preparation of specimens for X-ray fluorescence and X-ray diffraction analysis. Wiley-VCH, New York (1998)
23. Kumar, P., Sandhage, K.H: Near net-shaped magnesium aluminate spinel by the oxidation of solid magnesium-bearing precursors. Ceram. Trans. **94**, 129–140 (1998)
24. Deer, W.A., Howie, R.A., Zussman, J.: Rock-forming minerals. In: Framework silicates : feldspars, vol. 4A, 2nd edn. Geological Society of London Pub. House, Bath (2001)
25. Durinck, D., Arnout, S., Mertens, G., Boydens, E., Jones, P.T., Elsen, J., Blanpain, B., Wollants, P.: Borate distribution in stabilized stainless-steel slag. J. Am. Ceram. Soc. **91**(2), 548–554 (2008)
26. Craig J.R., Vaughan, D.J.: Ore microscopy and ore petrography—chapter 6. In: Quantitative Methods—Microindentation Hardness, 2nd edn. Wiley, New York (1994)
27. Barthelmy, D.: Mineralogy Database. Online at http://webmineral.com
28. http://www.liacs.nl/~jrijsdam/minerals/ (Accessed in November 2013)
29. Kim, Y.-M., Hong, S.-H.: Influence of minor ions on the stability and hydration rates of β-dicalcium silicate. J. Am. Ceram. Soc. **87**(5), 900–905 (2004). doi:10.1111/j.1551-2916.2004.00900.x
30. Ghosh, S.N., Rao, P.B., Paul, A.K., Raina, K.: Review. The chemistry of dicalcium silicate mineral. J. Mater. Sci. **14**(7), 1554–1566 (1979)
31. Juckes, L.M.: Dicalcium silicate in blast-furnace slag: A critical review of the implications for aggregate stability. Miner. Process. Extr. Metall. **111**(3), 120–128 (2002)
32. Chan, C.J., Kriven, M.W., Young, J.F.: Physical stabilization of the $\beta \rightarrow \gamma$ transformation in dicalcium silicate. J. Am. Ceram. Soc. **75**(6), 1621–1627 (1992)